applied sciences

MDPI

Article

Effect of Non-Metallic Inclusions on the Fatigue Strength Coefficient of High-Purity Constructional Steel Heated in Industrial Conditions

Tomasz Lipiński

Faculty of Technical Sciences, University of Warmia and Mazury in Olsztyn, 10-719 Olsztyn, Poland; tomaszlipinski.tl@gmail.com

Abstract: Steel fatigue strength testing is a process that requires large amounts of time, resources and appropriate equipment. The industry seeks to replace cumbersome destructive testing with non-destructive testing. Coefficients were developed that allow the comparison of the parameters of material properties. One such factor is the fatigue strength coefficient, which allows the estimate of fatigue strength using the known hardness of a given material. The fatigue strength factor should be developed for conditions that are as close to the industrial conditions as possible. It should take into account not only the expected properties of the material and the technological process but also its imperfections, e.g., the share of non-metallic inclusions and the steel microstructure. This paper presents the results of research on the influence of non-metallic inclusions on the fatigue strength coefficient of structural steel subjected to rotary bending. The tests were carried out in seven heats obtained in a 140-ton electric furnace under industrial conditions. The steel was desulfurized and refined with argon. The paper presents the bending fatigue strength of hardened and tempered steel at temperatures from 200 °C to 600 °C as a function of the relative volume of inclusions. The non-metallic inclusions occurring in steel were determined qualitatively and quantitatively. The derived fatigue strength coefficient, k, for different tempering temperatures makes it possible to estimate the fatigue strength of the analyzed steel as a function of its hardness for various microstructures represented by the respective tempering temperatures.

Keywords: steel; fatigue strength; non-metallic inclusion

Citation: Lipiński, T. Effect of Non-Metallic Inclusions on the Fatigue Strength Coefficient of High-Purity Constructional Steel Heated in Industrial Conditions. *Appl. Sci.* **2022**, *12*, 9292. https://doi.org/10.3390/app12189292

Academic Editor: José António Correia

Received: 26 August 2022
Accepted: 13 September 2022
Published: 16 September 2022

1. Introduction

There are elements of machines operating at variable stresses. These stresses can be regular or irregular. Ensuring a high reliability of elements operating under variable loads requires the use of steel with high fatigue strength [1–5]. Work is underway to understand the factors that reduce the fatigue life of the material [6–11]. One of the factors influencing the fatigue strength of steel, apart from the operating conditions, is non-metallic inclusions. There are many papers describing the influence of non-metallic inclusions on the development of microcracks and the fatigue strength of steel [12–17]. The rate of microcrack development under variable stress conditions is a determinant of the material's resistance to fatigue [18].

The problem of the impact of non-metallic inclusions in steel on its fatigue strength is complex. Steels operating under variable loads are usually high-quality steels. Fatigue strength tests of various types of steel used in industry are carried out [19,20]. Nevertheless, they have some amount of impurities. These impurities can significantly affect the properties of the material, in particular its fatigue strength. The shape, size, distribution, quality and quantity of non-metallic inclusions found in steel may vary depending on the manufacturing process [21–29].

Nodular inclusions are often observed in steels containing high levels of oxygen. The partial deoxidation of steel, e.g., with the addition of aluminum, favors the formation

of small oxide inclusions on the boundaries of austenite grains. On the other hand, the addition of an excess of deoxidizers may lead to the formation of large faceted inclusions. The influence of non-metallic inclusions on the fatigue strength is closely related to the processes taking place in micro-areas. The complexity of the problem results, among others, from local plastic deformation, cyclic strengthening and weakening, nucleation and the development and joining of microcracks [6,18,30–33].

Therefore, it is important to consider not only the behavior of individual structures and the morphology of inclusions but also their matrix, which is the steel microstructure [34–38].

There are many papers presenting the results of fatigue strength tests of hard materials (mainly bearing steels) and those produced on a laboratory scale [25,39–44]. It is much more difficult to find test results made on steel with high plasticity, which also justifies taking up the topic of this paper.

Steel fatigue tests are costly and time-consuming. For economic and time reasons, the industry conducts simulations more and more often to quickly estimate material properties, including fatigue strength [23,45,46]. There are known coefficients that allow for the estimation of fatigue strength as a function of static strength for specific conditions, such as Equation (1) [18,47]:

$$z_g = c \cdot R_m, \quad (1)$$

where:

z_g—fatigue strength, MPa;
c—coefficients of the equation;
R_m—tensile strength, MPa;
Therefore, Equation (2) can be written as:

$$c = z_g \cdot {R_m}^{-1}, \quad (2)$$

The industry strives to determine as many material properties as possible through non-destructive testing. Equation (3) was developed to estimate the tensile strength based on the results of non-destructive tests. The c_1 coefficient was introduced to compare the tensile strength to hardness:

$$R_m = c_1 \cdot HV, \quad (3)$$

where:

c_1—coefficients of the equation;
HV—Vickers hardness, MPa;
Then:

$$c = z_g \cdot (c_1 \cdot HV)^{-1}, \quad (4)$$

Expressing the coefficients c and c_1 with the coefficient k, we obtained Equation (5):

$$k = z_g \cdot HV^{-1}, \quad (5)$$

Many papers describe the effect of non-metallic inclusions on the fatigue strength of steel [11–30,48]. Unfortunately, the analysis of the impact of pollutants on the k coefficient determined by Equation (5) is not a popular area of study. However, it is a very useful method because it allows you to quickly estimate the fatigue strength, and the method is completely non-destructive.

The main purpose of this study was to determine the fatigue strength coefficients of various microstructures as a function of the relative contents of non-metallic inclusions and to determine the influence of the relative amounts of impurities on the fatigue strength coefficients of carbon steels with different tempering temperatures.

2. Materials and Methods

In order to determine the properties of the material that reaches recipients, it was decided to conduct the research on the material produced on an industrial scale. Carbon

steel used for machine elements operating at variable loads was analyzed. As the materials used for the elements of different machines must have different properties, it was decided to create different microstructures in the tested steel. For this purpose, it was decided to carry out hardening with tempering at different temperatures. This treatment ensured a hard microstructure of tempered martensite, an elastic microstructure of medium-tempered martensite and a plastic microstructure of highly tempered martensite.

The structural steel for the tests was heated in an industrial electric arc furnace with a capacity of 140 tons. The furnace input was pig iron with about 25% steel scrap. The tests were carried out in seven independent heats. The metal from the furnace was poured into a ladle with a capacity of 7 tons. The steel was desulfurized and then refined with argon. Argon was introduced into the ladle of liquid steel through a porous brick. The time of the refining process was established experimentally and was about 9 min. After the completion of the metal crystallization in the molds, it was rolled into billets with a diameter of 100 mm × 100 mm using conventional methods.

Samples were taken from the billets in order to determine: the chemical composition, metallographic studies, the relative volume of non-metallic inclusions and the phase composition of oxide inclusions. The contents of chemical elements in the steel were estimated using LECO analyzers, the AFL FICA quantometer and using conventional analytical methods. The relative volumes of non-metallic inclusions with dimensions of 2 µm and above were determined with a Quantimet videomicroscope at a magnification of 400×. The contents of non-metallic inclusions were determined separately for diameters of 2 µm and above, 5 µm and above, and 10 µm and above. The volume of all non-metallic inclusions was determined by chemical extraction methods. The relative volume of non-metallic inclusions with dimensions below 2 µm was determined analytically by determining the difference between the volume of all non-metallic inclusions and the volume of inclusions with a diameter of 2 µm or greater. The determination of the relative volume of inclusions was possible on the assumption that the quotient of the number of particles per area divided by the area was equal to the quotient of the number of particles in the volume divided by the volume. The volume of non-metallic inclusions in the Me-S system was lower than the error value in determining their share. For this reason, Me-S inclusions were excluded from further studies. Oxygen-based inclusions were thoroughly analyzed.

The real average chemical composition of the analyzed steel from seven heats is presented in Table 1.

Table 1. Average chemical composition of tested steel from seven temperatures (wt. %).

Chemical Element	C	Si	Mn	P	S	Cr	Ni	Mo	Cu	B
Contents	0.23	0.28	1.12	0.02	0.01	0.47	0.47	0.23	0.15	0.003
Standard deviation	0.017	0.047	0.123	0.004	0.004	0.058	0.040	0.016	0.014	0.001

Bars with a diameter of 10 mm were taken from the billets. The symmetry axes of the bars were parallel to the direction of the plastic processing of the material. The bars were austenitized for 30 min at 880 °C. Cooling was carried out in water. Then, the bars were tempered for 2 h at the following temperatures: 200 °C, 300 °C, 400 °C, 500 °C and 600 °C and cooled in air.

The average mechanical properties of the tested steel from seven heats, depending on the tempering temperature, are presented in Table 2.

The steel fatigue strength test was carried out on a VEB Werkstoffprufmaschinen rotary testing machine enabling rotary bending at 6000 rpm. A cylindrical sample with a constant cross-section of 10 mm in diameter was mounted in the rotating holders of the two-point loading testing machine. The tests were carried out in accordance with PN-74/H-04327 standards [49]. The samples were cut from 100 mm × 100 mm billets for each heat. The main axes of the rolls were parallel to the billet rolling direction. In order to determine the

fatigue strength of the steel, the tests were stopped after reaching 10^7 cycles. The load level during the fatigue tests was adjusted to the strength properties of the steel. In order for the samples to reach 10^4–10^6 cycles, characterizing the limits of fatigue strength, the load values were selected experimentally. The maximum loads during the test, depending on the tempering temperatures, are presented in Table 3.

Table 2. Average mechanical properties of tested steel from seven heats depending on the tempering temperature.

Tempering Temperature, °C	200	300	400	500	600
Tensile strength, MPa	1421	1347	1194	1073	887
Vickers hardness, HV	432	412	372	333	275

Table 3. Maximum loads during the test, depending on the tempering temperatures.

Tempering Temperature, °C	200	300	400	500	600
Maximum load, MPa	650	600	600	600	540

The fatigue strength coefficients for the tested tempering temperatures are presented in the form of linear regression equations of the general form (6):

$$k_{(tempering\ temp.)} = a \cdot V^2 + b \cdot V + c, \quad (6)$$

where:

$k_{(tempering\ temp.)}$—fatigue strength coefficient;

V—relative volume of non-metallic inclusions, vol. %;

a, b, c—coefficients of the equation.

The significance of the correlation coefficients, r, was determined on the basis of the critical value of the Student's t-distribution for a significance level of $\alpha = 0.05$ and the number of degrees of freedom of $f = n - 1$.

The dissipation coefficient $\delta_{(tempering\ temp.)}$ for the regression equation $k_{(tempering\ temp.)}$ was calculated using Equation (7):

$$\delta_{(tempering\ temp.)} = 2 \cdot s_k \cdot (1 - r^2)^{1/2}, \quad (7)$$

where:

s_k —standard deviation;

r—correlation coefficient.

3. Results

The non-metallic inclusion phase structure determined by the XRD method is shown in Table 4.

Table 4. Non-metallic inclusion phase structure (vol. %).

Statistical Parameter	Al_2O_3	SiO_2	CaO	MgO	MnO	Cr_2O_3	FeO
Arithmetic average	39.5	13.4	10.4	9.7	9.5	9.0	8.7
Standard deviation	2.021	1.437	1.470	0.962	0.215	1.174	3.057

Some of the non-metallic inclusions had a complex structure. The most common types of non-metallic inclusions occurring in the tested steel are shown in Figure 1.

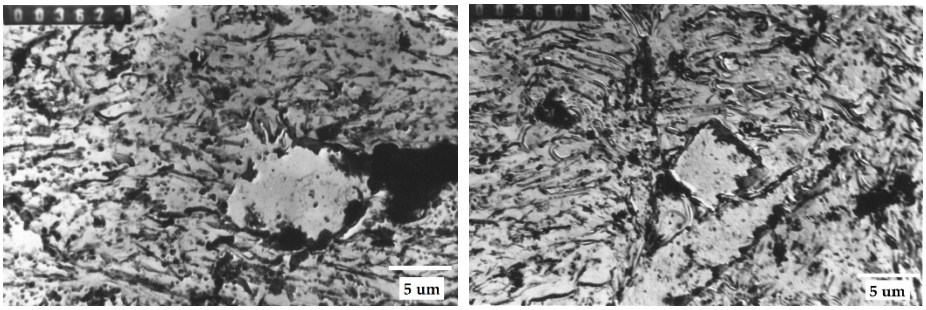

(**a**) (**b**)

Figure 1. Samples of non-metallic inclusion in research steel: (**a**) highly dispersive Al_2O_3 particles and multiphase inclusions (SiO_2·CaO) deformed during plastic working [50], (**b**) highly dispersive Al_2O_3 particles with the form of irregularly shaped polyhedra, Cr_2O_3 inclusions of a parallelepiped structure and SiO_2 inclusions deformed during plastic working.

The characteristics of the non-metallic inclusions of steel heated in an electric furnace and subjected to desulfurization and argon refining are presented using statistical parameters in Table 5.

The bending fatigue strength coefficient, *k*, of research steel after hardening and tempering at 200 °C depended on the relative content of non-metallic inclusions and is presented in Figure 2.

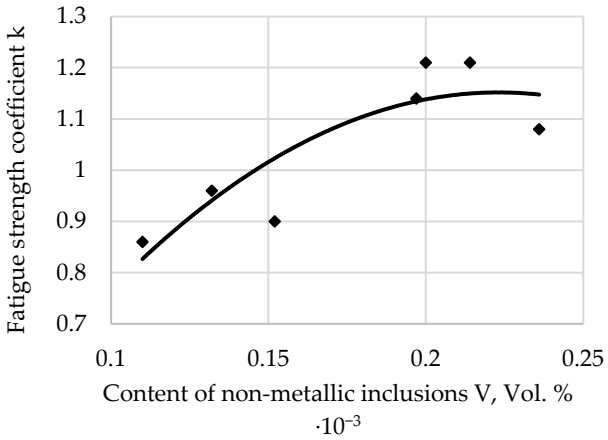

Figure 2. The bending fatigue strength coefficient, *k*, of research steel after hardening and tempering at 200 °C depends on the relative content of non-metallic inclusions.

The regression equation and the value of the correlation coefficient, *r*, are presented in Equation (8).

$$k_{(200)} = -25.397 \cdot V^2 + 11.334 \cdot V + 0.1128 \text{ and } r = 0.8736, \quad (8)$$

The bending fatigue strength coefficient, *k*, of research steel after hardening and tempering at 300 °C depends on the relative content of non-metallic inclusions and is presented in Figure 3.

Table 5. Characteristics of non-metallic inclusions.

	Relative Volume of Non-Metallic Inclusions, *V*, for Diameters, *d*, μm			
Statistical parameter	$V_0 < 2$	$V_2 > 2$	$V_5 > 5$	$V_{10} > 10$
Arithmetic average relative volume of non-metallic inclusions, Vol. %	0.077	0.100	0.080	0.046
Standard deviation	0.0124	0.0321	0.0234	0.0139

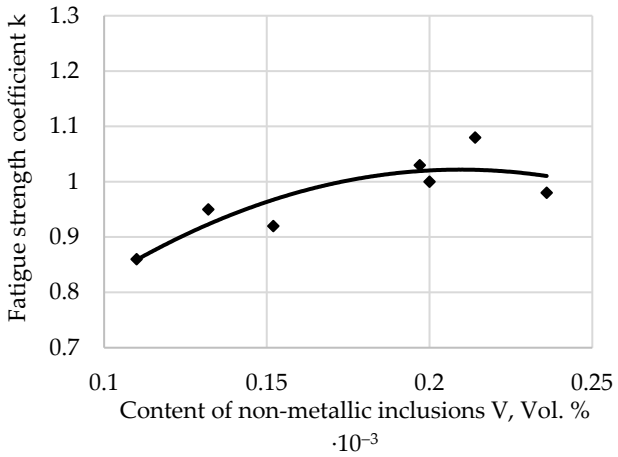

Figure 3. The bending fatigue strength coefficient, *k*, of research steel after hardening and tempering at 300 °C depends on the relative content of non-metallic inclusions.

The regression equation and the value of the correlation coefficient, *r*, is presented in Equation (9).

$$k_{(300)} = -16.477 \cdot V^2 + 6.904 \cdot V + 0.2986 \text{ and } r = 0.8668, \quad (9)$$

The bending fatigue strength coefficient, *k*, of research steel after hardening and tempering at 400 °C depends on the relative content of non-metallic inclusions and is presented in Figure 4.

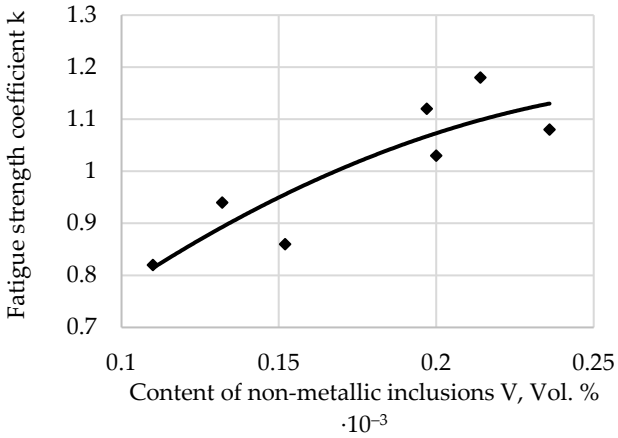

Figure 4. The bending fatigue strength coefficient, *k*, of research steel after hardening and tempering at 400 °C depends on the relative content of non-metallic inclusions.

The regression equation and the value of the correlation coefficient, *r*, are presented in Equation (10).

$$k_{(400)} = -10.246 \cdot V^2 + 6.053 \cdot V + 0.2721 \text{ and } r = 0.8773, \quad (10)$$

The bending fatigue strength coefficient, *k*, of research steel after hardening and tempering at 500 °C depends on the relative content of non-metallic inclusions and is presented in Figure 5.

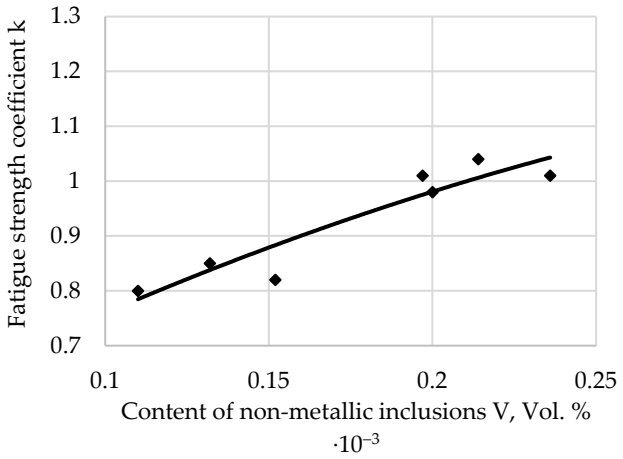

Figure 5. The bending fatigue strength coefficient, *k*, of research steel after hardening and tempering at 500 °C depends on the relative content of non-metallic inclusions.

The regression equation and the value of the correlation coefficient, *r*, are presented in Equation (11).

$$k_{(500)} = -3.5279 \cdot V^2 + 3.2719 \cdot V + 0.4674 \text{ and } r = 0.9354, \quad (11)$$

The bending fatigue strength coefficient, *k*, of research steel after hardening and tempering at 600 °C depends on the relative content of non-metallic inclusions and is presented in Figure 6.

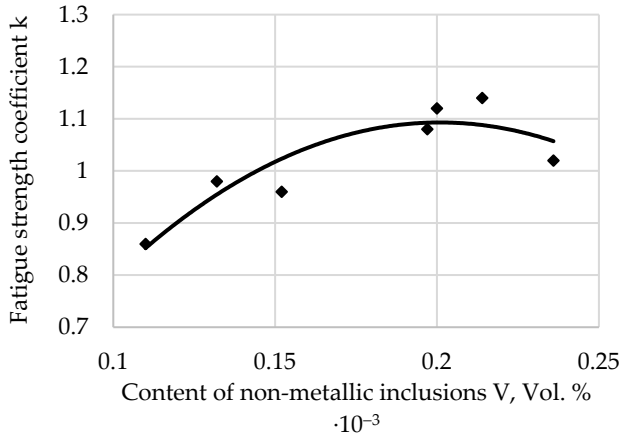

Figure 6. The bending fatigue strength coefficient, *k*, of research steel after hardening and tempering at 600 °C depends on the relative content of non-metallic inclusions.

The regression equation and the value of the correlation coefficient, *r*, are presented in Equation (12).

$$k_{(600)} = -29.154 \cdot V^2 + 11.716 \cdot V - 0.084 \text{ and } r = 0.9139, \quad (12)$$

The bending fatigue strength coefficient, *k*, of research steel after hardening and tempering for all tempering temperatures depends on the relative content of non-metallic inclusions and is presented in Figure 7.

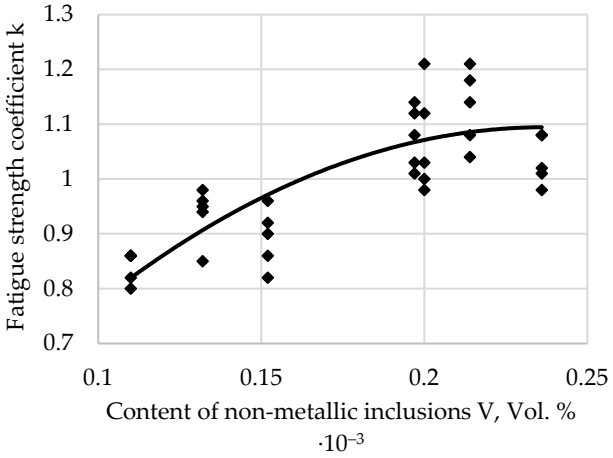

Figure 7. The bending fatigue strength coefficient, *k*, of research steel after hardening and tempering for all tempering temperatures depends on the relative content of non-metallic inclusions.

The regression equation and the value of the correlation coefficient, *r*, are presented in Equation (13).

$$k_{(all)} = -17.082 \cdot V^2 + 8.0935 \cdot V + 0.1357 \text{ and } r = 0.8101, \quad (13)$$

The statistical parameters representing the mathematical model (6), correlation coefficients and the degree of dissipation, *k*, around the regression line are presented in Table 6.

Table 6. Statistical parameters representing mathematical Equation (6), correlation coefficients and dissipation.

Tempering Temperature °C	Correlation Coefficient *r*	Degree of Dissipation, *k*, Around Regression Line (7)	$t_\alpha = 0.05$	$t_\alpha = 0.05$ from Student's Distribution for $p = (n - 1)$
200	0.8736	0.1415	4.3972	
300	0.8668	0.0723	4.2579	
400	0.8773	0.1470	4.4775	2.4469
500	0.9354	0.0724	6.4800	
600	0.9139	0.0803	5.5146	
all	0.8101	0.1360	8.0568	2.0452

4. Conclusions

The tested steel contained 0.23% C on average (Table 1). Therefore, it can be included in the group of low-carbon steels. Taking into account the standard deviation for the carbon content, it can be seen that the carbon content also exceeded the value of 0.25% C, which is an imaginary limit for classifying steels into the low-carbon and medium-carbon groups.

Qualitative and quantitative analyses of non-metallic inclusions showed the highest content of the Al_2O_3 phase, amounting to 39.5% by volume of all inclusions (Tables 4 and 5). The lower relative volumes of 13.4% and 10.4% were occupied by the SiO_2 phase and CaO, respectively. The volumes of the subsequent groups of non-metallic inclusions were determined to be at levels below 10%. Taking into account that the Al_2O_3 phase was present in the microstructure of the steel in the form of fine oval inclusions (Figure 1), it can be concluded that its amount is large. Other marked inclusions had much larger unit

volumes (dimensions). For all the tempering temperatures used, an increase in the fatigue strength coefficient was observed with an increase in the relative content of non-metallic inclusions (Figures 2–7). All equations describing the fatigue strength coefficient were statistically significant, which was confirmed by the analysis in Table 6. High reliability was obtained for all tested tempering temperatures. In general, as the tempering temperature increased, i.e., the ductility of the steel increased and its hardness and strength decreased, the correlation coefficient increased. Thus, for microstructures characterized by high plasticity, the presented regression equations are characterized by higher confidence. Such results can be explained by the fact that the brittle incision occurring in the hard matrix during fracture can form a notch favoring the propagation of the microcrack to the incision matrix. Moreover, the initial cracking of hard materials is easier than that of plastic materials [6,18]. Taking into account the random nature of inclusions in the volume of steel for materials with high hardness, it can be assumed that the formation of cracks initiated by these inclusions is also random. The highest reliability of the tested coefficient was noted for the tempering temperature of 500 °C.

Taking into account the results of this study and the studies presented in other papers [16,28,30], it can be assumed that, with a high proportion of submicroscopic inclusions, the value of the *k* coefficient increases with an increase in the relative content of non-metallic inclusions. This increase is explained by the shape and size of submicroscopic inclusions. The majority of these inclusions are aluminum oxides (Al_2O_3). Due to their small volume, they tend to keep the energy as low as possible. For this reason, their shape is similar to nodular. Assuming that they may constitute obstacles in the microstructure affecting the segmental slip bands, the deformation blockade effect by sub-boundaries may occur. The collapse of the slip bands at the inclusion–matrix phase sub-boundary forces the possibility of crossing the obstacle and the activation of the sources of slip lying on the other side of the slip boundary. The formation of twins may cause a change in the course of material fatigue and thus may also delay the formation of microcracks in a material with sufficiently high plasticity. The above mechanism seems to be more possible the more plastic the matrix of non-metallic inclusions is (higher tempering temperature of steel). In the case of large precipitates (over 10 μm) in the microstructure, they can act as notches. Especially if they have low durability.

Based on the conducted industrial research, the following were determined:

1. Fatigue strength coefficients for various microstructures in the function relative content of non-metallic inclusions;
2. Qualitatively and quantitatively analyzed the occurrence of steel non-metallic inclusions;
3. The influence of the relative amount of non-metallic inclusions on the fatigue strength factor of carbon steels with different tempering temperatures.

Funding: This research received no external funding.

Institutional Review Board Statement: Not applicable.

Informed Consent Statement: Not applicable.

Conflicts of Interest: The authors declare no conflict of interest.

References

1. Kłysz, S. Selected problems of fatigue of materials and constructions elements. *Tech. Sci.* **2005**, *8*, 141–164.
2. Kováčiková, P.; Dubec, A.; Kuricová, J. The microstructural study of a damaged motorcycle gear wheel. *Manuf. Technol.* **2021**, *21*, 83–90. [CrossRef]
3. Blikharskyy, Y.; Selejdak, J.; Kopiika, N. Corrosion fatigue damages of rebars under loading in time. *Materials* **2021**, *14*, 3416. [CrossRef]
4. Hren, I.; Michna, Š.; Novotný, J.; Michnová, L. Comprehensive analysis of the coated component from a FORD engine. *Manuf. Technol.* **2021**, *21*, 464–470. [CrossRef]
5. Jopek, M. Determination of Carbon Steel Dynamic Properties. *Manuf. Technol.* **2021**, *21*, 479–482. [CrossRef]
6. Suresh, S. *Fatigue of Materials*; Cambridge University Press: Cambridge, UK, 1998.

7. Lenkovskiy, T.M.; Kulyk, V.V.; Duriagina, Z.A.; Kovalchuk, R.A.; Topilnytskyy, V.H.; Vira, V.V.; Tepla, T.L. Mode I and mode II fatigue crack growth resistance characteristics of high tempered 65G steel. *Arch. Mater. Sci. Eng.* **2017**, *84*, 34–41. [CrossRef]
8. Malashchenko, V.; Strilets, O.; Strilets, V.; Kłysz, S. Investigation of the energy effectiveness of multistage differential gears when the speed is changed by the carrier. *Diagnostyka* **2019**, *20*, 57–64. [CrossRef]
9. Halford, G.L. *Low Cycle Thermal Fatigue*; NASA: Washington, DC, USA, 1986.
10. Blikharskyy, Z.; Brózda, K.; Selejdak, J. Effectivenes of Strengthening Loaded RC Beams with FRCM System. *Arch. Civ. Eng.* **2018**, *64*, 3–13. [CrossRef]
11. Milovanovi´c, V.; Duni´c, V.; Raki´c, D.; Živkovi'c, M. Identification causes of cracking on the underframe of wagon for containers transportation—fatigue strength assessment of wagon welded joints. *Eng. Fail. Anal.* **2013**, *31*, 118–131. [CrossRef]
12. Roiko, A.; Hänninen, H.; Vuorikari, H. Anisotropic distribution of non-metallic inclusions in forged steel roll and its influence on fatigue limit. *Int. J. Fatigue* **2012**, *41*, 158–167. [CrossRef]
13. Lipiński, T.; Ulewicz, R. The effect of the impurities spaces on the quality of structural steel working at variable loads. *Open Eng.* **2021**, *11*, 233–238. [CrossRef]
14. Spriestersbach, D.; Grad, P.; Kerscher, E. Influence of different non-metallic inclusion types on the crack initiation in high-strength steels in the VHCF regime. *Int. J. Fatigue* **2014**, *64*, 114–120. [CrossRef]
15. Lipiński, T.; Wach, A.; Detyna, E. Influence of Large Non-Metallic Inclusions on Bending Fatigue Strength Hardened and Tempered Steels. *Adv. Mater. Sci.* **2015**, *15*, 33–40. [CrossRef]
16. Zhao, Y.; Li, T.; Tang, G.; Gup, H.; Yan, J.; Gou, X.; Zhu, Y. Characterization of the morphological evolution of MnS inclusions in free-cutting steel during heating. *J. Mater. Res. Technol.* **2022**, *17*, 1427–1437. [CrossRef]
17. Lipiński, T.; Wach, A. The effect of fine non-metallic inclusions on the fatigue strength of structural steel Terms and conditions. *Arch. Metall. Mater.* **2015**, *60*, 65–69. [CrossRef]
18. Kocańda, S. *Fatigue Failure of Metals*; WNT Warsaw Poland: Warsaw, Poland, 1985. (In Polish)
19. Milovanović, V.; Arsić, D.; Milutinović, M.; Živković, M.; Topalović, M.A. Comparison Study of Fatigue Behavior of S355J2+N, S690QL and X37CrMoV5-1 Steel. *Metals* **2022**, *12*, 1199. [CrossRef]
20. Ulewicz, R.; Szataniak, P.; Novy, F.; Trsko, L.; Bokuvka, O. Fatigue Characteristics of Structural Steels in the Gigacycle Region of Loading. Mater. *Today Proc.* **2017**, *4*, 5979–5984.
21. Beretta, S.; Murakami, Y. Largest-Extreme-Value Distribution Analysis of Multiple Inclusion Types in Determining Steel Cleanliness. *Metall. Mater. Trans.* **2001**, *32B*, 517–523. [CrossRef]
22. Jonšta, P.; Jonšta, Z.; Brožová, S.; Ingaldi, M.; Pietraszek, J.; Klimecka-Tatar, D. The Effect of Rare Earth Metals Alloying on the Internal Quality of Industrially Produced Heavy Steel Forgings. *Materials* **2021**, *14*, 5160. [CrossRef]
23. Lipiński, T.; Wach, A. Influence of outside furnace treatment on purity medium carbon steel. In Proceedings of the METAL 2014—23rd International Conference on Metallurgy and Materials, Brno, Czech Republic, 21–23 May 2014; pp. 738–743.
24. Podorska, D.; Drożdż, P.; Falkus, J.; Wypartowicz, J. Calculations of oxide inclusions composition in the steel deoxidized with Mn, Si and Ti. *Arch. Metall. Mater.* **2006**, *51*, 581–586.
25. Lipiński, T.; Wach, A. Dimensional Structure of Non-Metallic Inclusions in High-Grade Medium Carbon Steel Melted in an Electric Furnace and Subjected to Desulfurization. *Solid State Phenom.* **2015**, *223*, 46–53. [CrossRef]
26. Hua, L.; Deng, S.; Han, X.; Huang, S. Effect of material defects on crack initiation under rolling contact fatigue in a bearing ring. *Tribol. Int.* **2013**, *66*, 315–323. [CrossRef]
27. Gulyakov, V.S.; Vusikhis, A.S.; Kudinov, D.Z. Nonmetallic Oxide Inclusions and Oxygen in the Vacuum_Jet Refining of Steel. *Steel Transl.* **2012**, *42*, 781–783. [CrossRef]
28. Murakami, Y.; Kodama, S.; Konuma, S. Quantitative evaluation of effects of non-metallic inclusions on fatigue strength of high strength steels, I: Basic fatigue mechanism and fatigue fracture stress and the size and location of non-metallic inclusions. *Int. J. Fatigue* **1989**, *11*, 291–298. [CrossRef]
29. Srivastava, A.; Ponson, L.; Osovski, S.; Bouchaud, E.; Tvergaard, V.; Needleman, A. Effect of inclusion density on ductile fracture toughness and roughness. *J. Mech. Phys. Solids* **2014**, *63*, 62–79. [CrossRef]
30. Yang, Z.G.; Zhang, J.M.; Li, S.X.; Li, G.Y.; Wang, Q.Y.; Hui, W.J.; Weng, Y.Q. On the critical inclusion size of high strength steels under ultra-high cycle fatigue. *Mater. Sci. Eng. A* **2006**, *427*, 167–174. [CrossRef]
31. Lipiński, T. Effect of the spacing between submicroscopic oxide impurities on the fatigue strength of structural steel. *Arch. Metall. Mater.* **2015**, *60*, 2385–2390. [CrossRef]
32. Qayyum, F.; Umar, M.; Elagin, V.; Kirschner, M.; Hoffmann, F.; Guk, S.; Prahl, U. Influence of non-metallic inclusions on local deformation and damage behavior of modified 16MnCrS5 steel. *Crystals* **2022**, *12*, 281. [CrossRef]
33. Lipiński, T. The effect of the diameter and spacing between impurities on the fatigue strength coefficient of structural steel. *Arch. Metall. Mater.* **2018**, *63*, 519–524.
34. Chan, K.S. Roles of microstructure in fatigue crack initiation. *Int. J. Fatigue* **2010**, *32*, 1428–1447. [CrossRef]
35. Dobrzański, L.A. Heat treatment as the fundamental technological process of formation of structure and properties of the metallic engineering materials. In Proceedings of the 8th Seminar of the International Federation for Heat Treatment and Surface Engineering IFHTSE, Dubrovnik-Cavtat, Croatia, 12–14 September 2001; pp. 1–12.
36. Macek, W.; Szala, M.; Trembacz, J.; Branco, R.; Costa, J. Effect of non-zero mean stress bending-torsion fatigue on fracture surface parameters of 34CrNiMo6 steel notched bars. *Prod. Eng. Arch.* **2020**, *26*, 167–173. [CrossRef]

37. Zhang, G.; Zhang, Q.; Yang, J.; Xie, Z.; Zhang, L.; Liu, R.; Li, G.; Wang, H.; Fang, Q.; Wang, X. Microstructures and Tensile Properties of 9Cr-F/M Steel at Elevated Temperatures. *Materials* **2022**, *15*, 1248. [CrossRef] [PubMed]
38. Mousavi, S.M.; Paavola, J. Analysis of a cracked concrete containing an inclusion within homogeneously imperfect interface. *Mech. Res. Commun.* **2015**, *63*, 1–5. [CrossRef]
39. Dong, Z.; Qian, D.; Yin, F.; Wang, F. Enhanced Impact Toughness of Previously Cold Rolled High-Carbon Chromium Bearing Steel with Rare Earth Addition. *J. Mater. Eng. Perform.* **2021**, *30*, 8178–8187. [CrossRef]
40. Ossola, E.; Pagliassotto, S.; Rizzo, S.; Sesana, R. Microinclusion and Fatigue Performance of Bearing Rolling Elements. In *Mechanical Fatigue of Metals: Experimental and Simulation Perspectives*; Springer: Berlin/Heidelberg, Germany, 2019; Volume 7, pp. 321–326.
41. Melander, A.; Rolfsson, M.; Nordgren, A.; Jansson, B.; Hedberg, H.; Lund, T. Influence of inclusion contents on fatigue properties of SAE-52100 bearing steels. *Scand. J. Metall.* **1991**, *20*, 229–244.
42. Zhou, D.G.; Fu, J.; Chen, X.C.; Li, J. Study on oxygen content, inclusions and fatigue properties of bearing steels produced by different processes. *J. Univ. Sci. Technol. Beijing* **2001**, *8*, 25–27.
43. Gu, C.; Liu, W.Q.; Lian, J.H.; Bao, Y.P. In-depth analysis of the fatigue mechanism induced by inclusions for high-strength bearing steels. *Int. J. Miner. Metall. Mater.* **2021**, *28*, 826–834. [CrossRef]
44. Shi, Z.Y.; Li, J.J.; Zhang, X.D.; Shang, C.J.; Cao, W.Q. Influence Mechanisms of Inclusion Types on Rotating Bending Fatigue Properties of SAE52100 Bearing Steel. *Materials* **2022**, *15*, 5037. [CrossRef]
45. Anderson, C.W.; Shi, G.; Atkinson, H.V.; Sellars, C.M. The precision of methods using the statistics of extremes for the estimation of the maximum size of inclusions in clean steels. *Acta Mater.* **2000**, *48*, 4235–4246. [CrossRef]
46. Krynke, M. Management optimizing the costs and duration time of the process in the production system. *Prod. Eng. Arch.* **2021**, *27*, 163–170. [CrossRef]
47. Guide engineer. *Mechanic*; Scientific and Technical Publishing: Warsaw, Poland, 1970. (In Polish)
48. Lipiński, T.; Wach, A. Influence of inclusions on bending fatigue strength coefficient the medium carbon steel melted in an electric furnace. *Prod. Eng. Arch.* **2020**, *26*, 86–91. [CrossRef]
49. PN-74/H-04327. Metals Testing for Fatigue. Axial Tensile-Compression Test at a Constant Cycle of External Loads. Polish Standards: Warsaw, Poland, 1974.
50. Lipiński, T.; Wach, A. The Share of Non-Metallic Inclusions in High-Grade Steel for Machine Parts. *Arch. Foundry Eng.* **2010**, *10*, 45–48.